



Numerical Investigation of Fluid Flow Mechanism in the Back Shroud Cavity of a Centrifugal Pump

W. Dong¹ and W. L. Chu^{1,2}

¹ School of Power and Energy, Northwestern Polytechnical University, Xi'an 710129, China

² Collaborative Innovation Center of Advanced Aero-Engine, Beijing, 100191, China

†Corresponding Author Email: 735381559@qq.com

(Received February 28, 2017; accepted December 23, 2017)

ABSTRACT

A detailed analysis on the fluid flow distribution in the back shroud cavity is significant for accurately calculating axial forces in the operation of centrifugal pumps. The numerical calculation results and the experimental results were basically consistent on the performance of the centrifugal pump and the fluid flow characteristics in the back shroud cavity. Distribution of velocity field was researched in the back shroud cavity. We plot the axial distribution curves of the dimensionless circumferential and radial components of velocity of the fluid inside the cavity with different angles and radii. We then analyze the fluid pressure distribution in the back shroud cavity and compare it with experimental results. Results show that the fluid flow in the back shroud cavity involves the core area and the fluid leakage. Results also show that the fluid in the core area behaves like a revolving rigid body. At the operating points of the same flow rate, the cross-sectional area of the volute directly affects the flow rate of the fluid in the back shroud cavity, significantly restricting the fluid flow in that component. However, the flow pattern in the turbulent boundary layer is strongly affected by the leakage flow; hence, the distribution of velocity is not axially symmetric. When the flow rate increases from 0.8 Q_{sp} to 1.2 Q_{sp} , the radial differential pressure between the sealing ring and the volute decreases. Meanwhile, the disc friction loss of the impeller-to-wall inside the back shroud cavity tends to be more circumferentially or radially equal, whereas the radial leakage rate in the back shroud cavity tends to decrease. The fluid flow in the back shroud cavity comprises the circumferential shear flow and radial differential pressure flow and is considered as a 2D viscous laminar flow.

Keywords: Centrifugal pump; Back shroud cavity; Circumferential velocity component; Radial velocity component; Pressure.

NOMENCLATURE

b	sealing ring radial clearance	\bar{v}_u	dimensionless circumferential velocity component
d	balance hole diameter	\bar{v}_r	dimensionless radial velocity component
D	shroud diameter	z_1	balance holes number
D_n	front sealing ring diameter	r_2	blade number
D_m	back sealing ring diameter	v_u	circumferential velocity component of the measuring point in the cavity
H	head	v_r	radial velocity component of the measuring point in the cavity
H	efficiency	ω	angular velocity of the impeller
n	rotating speed	δ	axial clearance of the back shroud cavity
n_s	specific speed	s	axial distance from the measuring point to the outer side wall face of impeller back shroud
Q_{sp}	design flow rate		
r	radius of the measuring point in the cavity		
R	shroud radius		
\bar{s}	dimensionless axial length factor		

1. INTRODUCTION

Axial forces exist in pump operations and affect the safety and stability of centrifugal pumps. Therefore, calculating and balancing the axial forces has long been an important and complex problem in research on pump operations. 10 or more empirical and semi-empirical formulas are commonly used to calculate the axial force of the centrifugal pump based on the hypothesis that no leakage flow occurs in the shroud cavity and that the angular velocity of fluid in the back shroud cavity is half of the impeller (Shimura *et al.* 2012, Mou *et al.* 2010). In (Verba and Sebestyem 1966, Lino *et al.* 1980), experimental studies have shown that the ratio k of the angular velocity of the fluid in the back shroud cavity to the impeller rotation angle is inconsistent with the aforementioned hypothesis and that the axial force calculated based on the hypothesis is much smaller than the measured value of the multistage pump. Based on the mathematical-physical model of the flow characteristics in the shroud cavity of the centrifugal pump established in (Yang *et al.* 2003), the fluid in the back shroud cavity, the tangential velocity, and the radial velocity were calculated by different Reynolds numbers and leakage values; the resultant angular velocity of fluid in the back shroud cavity was 48% of the impeller. In (Wang *et al.* 2009), the structural characteristics of the back shroud cavity of the centrifugal pump under the design condition were numerically simulated, and the results showed that the flow field distribution in the cavity was axially asymmetric. Furthermore, the flow field structure was more complex than that inside the closed casing of the rotor and stator, although they both showed similar axial variations in the flow field.

Many scholars have studied the fluid flow characteristics in the cavity, but none of their studies have provided detailed distribution characteristics of fluid flow in the cavity with different angles and radii. In (Benigni *et al.* 2012), the numerical simulations are used to predict the performance of centrifugal pumps and found that fluid flow characteristics in the cavity strongly influenced the accuracy and precision of the results. The acting force of the back shroud was an essential component of the axial force of the centrifugal pump (Guan 2011, Dong *et al.* 2016). Therefore, the fluid flow characteristics in the cavity directly affect the performance of the centrifugal pump and the acting force of the back shroud. A detailed analysis on the fluid flow distribution in the back shroud cavity is essential to predicting accurately the performance of the centrifugal pump and calculating the axial force.

In this paper, a numerical simulation on the flow field is conducted for the entire flow path of an IS150–125–315 single-stage single-suction centrifugal pump. In addition, based on the consistency between the numerical simulation and experimental results of the pump performance and the fluid flow rate in the back shroud cavity, the axial variations of the fluid inside the back shroud cavity in the dimensionless circumferential and radial components of velocity are explored at the pump flow rates of 0.8, 1.0, and 1.2 Q_{sp} and with different angles (0° , 90° , 180° , and 270°) and radii (0.6, 0.7, 0.8, and 0.9R). Then the accuracy of

the numerical analysis is validated by comparing the numerical simulation and experimental results of the fluid pressure distribution in the back shroud cavity.

2. RESEARCH MODELS AND CALCULATION METHOD

2.1 Model Pump

The design parameters for this pump are presented in Table 1.

Pro/E software is used for geometric modeling. Auxiliary computational domains are added at the impeller inlet and the volute outlet, fully developing the outflow fluid and forming a solid model, as shown in Fig. 1.

Table 1 The design parameters of the pump

Description	Parameter	Value
Design flow rate (m ³ /h)	Q_{sp}	200
Head (m)	H	32
Rotating speed (r/min)	n	1450
Specific speed	n_s	87
Shroud diameter (mm)	D	325
Front sealing ring diameter (mm)	D_n	140
Back sealing ring diameter (mm)	D_m	165
Sealing ring radial clearance (mm)	b	0.22
Balance hole diameter (mm)	d	8
Balance holes number	z_1	6
Blade number	z_2	6

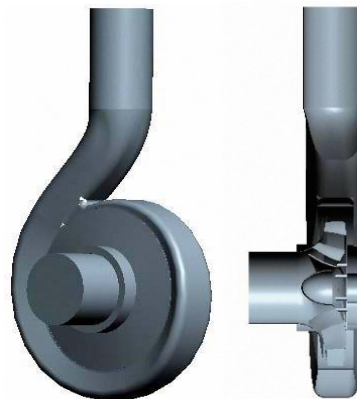


Fig. 1. Full port geometric model.

GAMBIT2.4 software is used for the computational domain meshing. Flexible and adaptive hybrid meshes are typically used to solve complicated boundary problems. Therefore, the model in this paper adopts hybrid meshes, as shown in Fig. 2. The structurally complex model of impeller passage, volute, and front cavity adopts tetrahedral meshes, whereas the structurally complex model of the back shroud cavity, seal ring clearance, and auxiliary computational domain adopts hexahedral meshes. The total number of cells is 1.94×10^6 . Table 2 displays the meshing-

independent validation results of the centrifugal pump at design flow rate (Q_{sp}). The results are presented independently from the meshing to eliminate the effects of the number of cells on the simulation results.



Fig. 2. Computational Mesh model.

Table 2 Grid independence check

Number of cells	Efficiency	Head/(m)	Power/(kW)
1.10×10^6	0.8176	33.02	21.99
1.94×10^6	0.8280	32.85	21.60
3.00×10^6	0.8274	32.84	21.62

In Table 2, when the number of cells increases from 1,100,000 to 1,940,000, the relative efficiency, head, and power error rates are 1.26%, 0.52%, and 1.81%, respectively; and when the number of cells increases from 1,940,000 to 3,000,000, the relative efficiency, head, and power error rates are 0.07%, 0.03% and 0.09%, respectively. Therefore, a cell-independent solution can be obtained when the number of cells is 1,940,000. In this paper, the computational model adopts 1,940,000 cells.

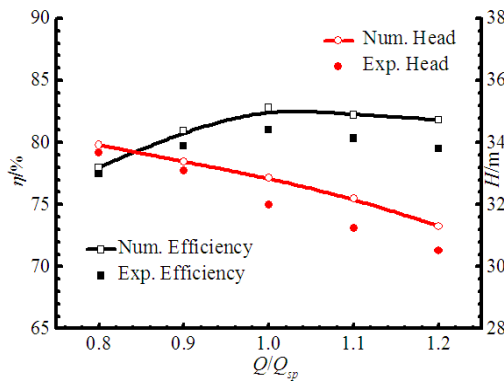
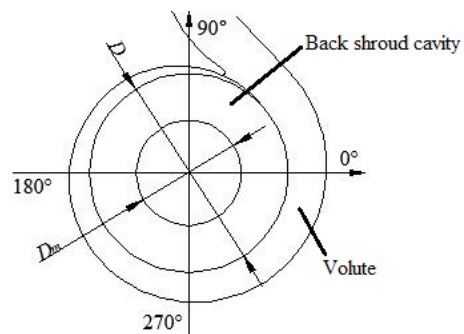


Fig. 3. Performance curves of the centrifugal pump.

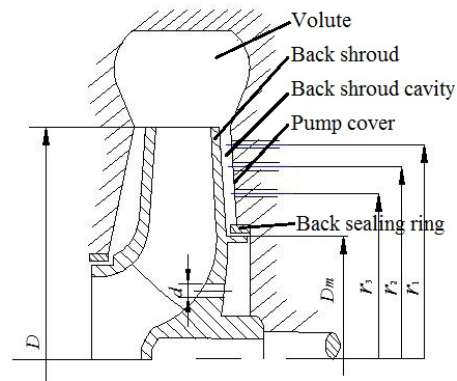
In Fig. 3, at the work area 0.8–1.2 Q_{sp} , the numerical

simulation results of the head and efficiency of the centrifugal pump are consistent with the experimental results. At the operating point with a design flow of 1.0 Q_{sp} , the numerical simulation results of efficiency are higher than those of the experimental results and have a relative error of 2.22%; furthermore, the numerical simulation results of the head are greater than those of the experimental results and have a relative error of 2.66%. Thus, the numerical simulation results of the performance of the pump are consistent with the experimental results and satisfy the research requirements in this paper.

The impeller inlet faces the positive z -axis direction during modeling and rotates clockwise. To facilitate the analysis on the distribution of the fluid flow in the back shroud cavity, the positive x -axis direction is defined as 0° and the positive y -axis direction is defined as 90° , as shown in Fig. 4.



(a) Circumferential view of the centrifugal pump



(b) Meridional plane of the centrifugal pump

Fig. 4. Schematic diagrams of the computational model.

2.2 Numerical Method

Numerical calculations are performed using FLUENT software. Boundary conditions were set as follows: the pump inlet was set as the velocity entrance without swirl flow, and the pump outlet was set as the free outflow pattern. Assuming that non-slip occur on the solid wall surfaces of the blade surface and volute, the wall function method was utilized to deal with the near-wall turbulence flow. Given that the working medium in the centrifugal pump is clean water, the flow in the pump body was set as incompressible

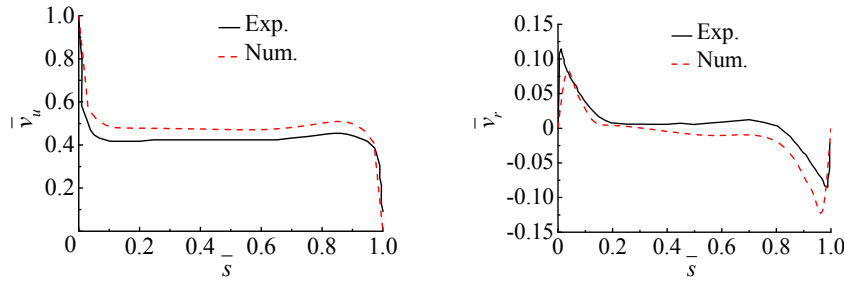


Fig. 5. Comparison of numerical and experimental results.

turbulent flow with constant physical property. Accordingly, the RNG $k-\varepsilon$ turbulence model was adopted, and a SIMPLEC algorithm was used to deal with the coupling between pressure and velocity. Difference schemes were set as follows: the pressure sub-relaxation item is in the standard format, and the momentum sub-relaxation item, turbulent energy sub-relaxation item, turbulent energy dissipation sub-relaxation item, and turbulent energy dissipation rate are all Second-order Upwind Difference Scheme dispersion difference equations. The following are the coefficients in the iterative calculation of algebraic equations: the sub-relaxation coefficient for pressure, which is 0.3; the momentum, which is 0.7; the turbulence energy, which is 0.8; and the turbulence energy dissipation rate, which is 0.8.

3. NUMERICAL METHOD VALIDATION

In (Itoh *et al.* 1992), numerous experimental data were obtained by using a hot-wire anemometer to measure the velocity distribution of the turbulent flow field on the rotating disc inside the closed cylinder. In (Pan *et al.* 2009), the particle image velocimetry (PIV) test results and the hot-wire measurement data were compared, and they found that the distributions of the circumferential and radial components of velocity were consistent at the radial geometrical center of the disc (0.6–0.8) R . At the cavity zone 0.8 R of the pump close to the radial geometrical center of the cavity, the fluid flow was less affected by the leakage flow and was approximated as the flow on the rotating disc inside the closed cylinder. In (Itoh *et al.* 1992), the experimental data at 0.8 R were compared with the axial distribution curves of the circumferential and radial components of velocity at the design flow point 0.8 R inside the back shroud cavity, as illustrated in Fig. 5. A dimensionless quantity is introduced to facilitate the analysis on the relationship between the flow rate in the cavity and the rotational speed of the impeller. The axial distribution curves of the circumferential and radial components of velocity will be analyzed as follows.

$$\bar{v}_u = \frac{v_u}{u_{ref}} \quad (1)$$

$$\bar{v}_r = \frac{v_r}{v_{ref}} \quad (2)$$

$$\bar{s} = \frac{s}{\delta} \quad (3)$$

Where $u_{ref} = \omega r$, \bar{v}_u is dimensionless circumferential

velocity component, \bar{v}_r is dimensionless radial velocity component, \bar{s} is dimensionless axial length factor, v_u is circumferential velocity component of the measuring point in the cavity (m/s), v_r is radial velocity component of the measuring point in the cavity (m/s), r is radius of the measuring point in the cavity (m), ω is angular velocity of the impeller (rad/s), δ is axial clearance of the back shroud cavity (m), s is axial distance from the measuring point to the outer side wall face of impeller back shroud (m).

In Fig. 5, the simulation results of the axial distribution curves of the circumferential and radial velocities of the fluid flow in the back shroud cavity are consistent with the changing trend of the experimental results. Considering the viscous effect of the fluid, turbulent boundary layers still exist near the outer face of the back shroud of the rotary impeller and the inner face of the stationary pump cover. Moreover, almost no axial change is observed in the core area of the flow between the boundary layers (Itoh *et al.* 1992, Pan *et al.* 2009, Park *et al.* 2009). Given the presence of the radial fluid flow, the back shroud cavity can obtain a high-energy fluid from the volute, leading to a circumferential component of velocity in the back shroud cavity that is slightly larger than the measured circumferential component of velocity on the rotating disc. The radial leakage rate near the face of the pump cover also increases slightly; thus, certain deviations are noticed between the experimental results and the axial distribution curves of the simulation results. Nonetheless, the overall changing trends of the circumferential and radial components of velocity in the back shroud cavity are not affected. These results indicate that the calculation method in this paper is feasible and can reflect the characteristics of fluid flow inside the back shroud cavity.

4. CHARACTERISTICS OF FLUID FLOW IN THE BACK SHROUD CAVITY

4.1 Velocity Distributions

Figure 6 contains the absolute velocity distributions of the fluid in the back shroud cavity along the outer face of the back shroud, the axial central section of the cavity, and the inner face of the pump cover at the operating points with the flow rates of 0.8, 1.0, and 1.2 Q_{sp} .

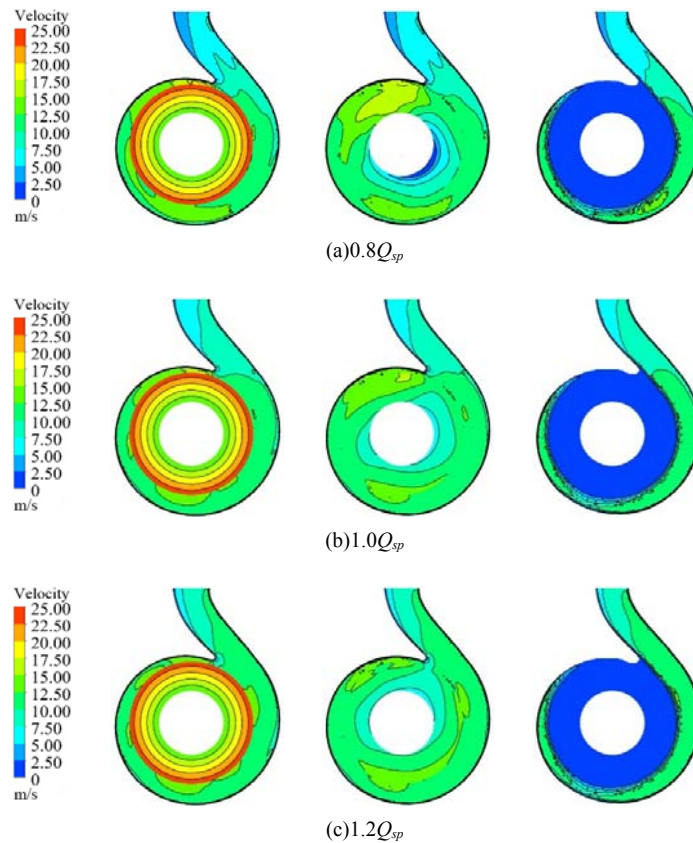


Fig. 6. Circumferential view of absolute velocity in the back shroud cavity.

In Fig. 6, at operating points of the same flow rate, from the inner diameter of the back shroud cavity to the outer diameter, the absolute velocity on the face of the impeller cap becomes radially larger and remains tangentially unchanged, on the back shroud cavity near the pump cover is zero. On the axial central section of the cavity is affected by the mainstream flow in the volute, the angular velocity of the impeller, the radial leakage flow, and the flow on the pump cover face, without any circumferentially stable fluid flow formed inside the cavity. This process results in an uneven velocity distribution in the cavity and complex circumferential and radial variations without axial symmetry in the absolute velocity. This result indicates that the impeller cap face rotates by the rated speed of the impeller, whereas the pump cover remains static. When the flow rate increases from $0.8 Q_{sp}$ to $1.2 Q_{sp}$, the rate in the high-speed flow zone of the cavity close to the volute tongue decreases and the rate in the low-speed flow zone close to the sealing ring increases. Therefore, the field distribution of the absolute velocity of the fluid in the back shroud cavity is consistent with the actual flow situation inside the pump, validating the reliability of this model for analyzing the characteristics of fluid flow inside the back shroud cavity.

4.2 Analysis of Fluid Flow

This study uses the analyses above to study the axial distribution curves of the circumferential and

radial velocities in the back shroud cavity at flow rates of 0.8, 1.0, and $1.2 Q_{sp}$; by angles of 0° , 90° , 180° , and 270° ; and with radii of 0.6, 0.7, 0.8, and $0.9R$ ($R=D/2$), as presented in Figs. 7 and 8.

In Figs. 7 and 8, turbulent boundary layers still exist in the cavity flow rate of the pump, close to the outer face of the back shroud of the rotary impeller, and in the stationary inner face of the pump cover. The core area between the boundary layers displayed negligible axial change (Lefor *et al.* 2014, Gülich *et al.* 2003).

In Fig. 7, at the low-flow operating point ($0.8 Q_{sp}$), a high differential pressure between the sealing ring and the volute is observed, and the sectional areas of the volute by the angles of 0° and 270° are large. The fluid in the back shroud cavity continuously transports the fluid with high kinetic energy into the volute along the impeller cap face, resulting in a reduction of kinetic energy in the directions of 0° and 270° while increasing the pressure potential energy. The circumferential velocity increases with the radius in the core zone fluid. The sectional areas of the volute in the directions of 90° and 180° are relatively small, resulting in a large kinetic energy of the fluid in the directions of 90° and 180° with low pressure potential energy. At the smaller radius, the kinetic energy of the fluid increases most notably, and at the radii of 0.6, 0.7, 0.8, and $0.9R$ (in the radial direction), the larger the radius, the smaller the circumferential velocity in

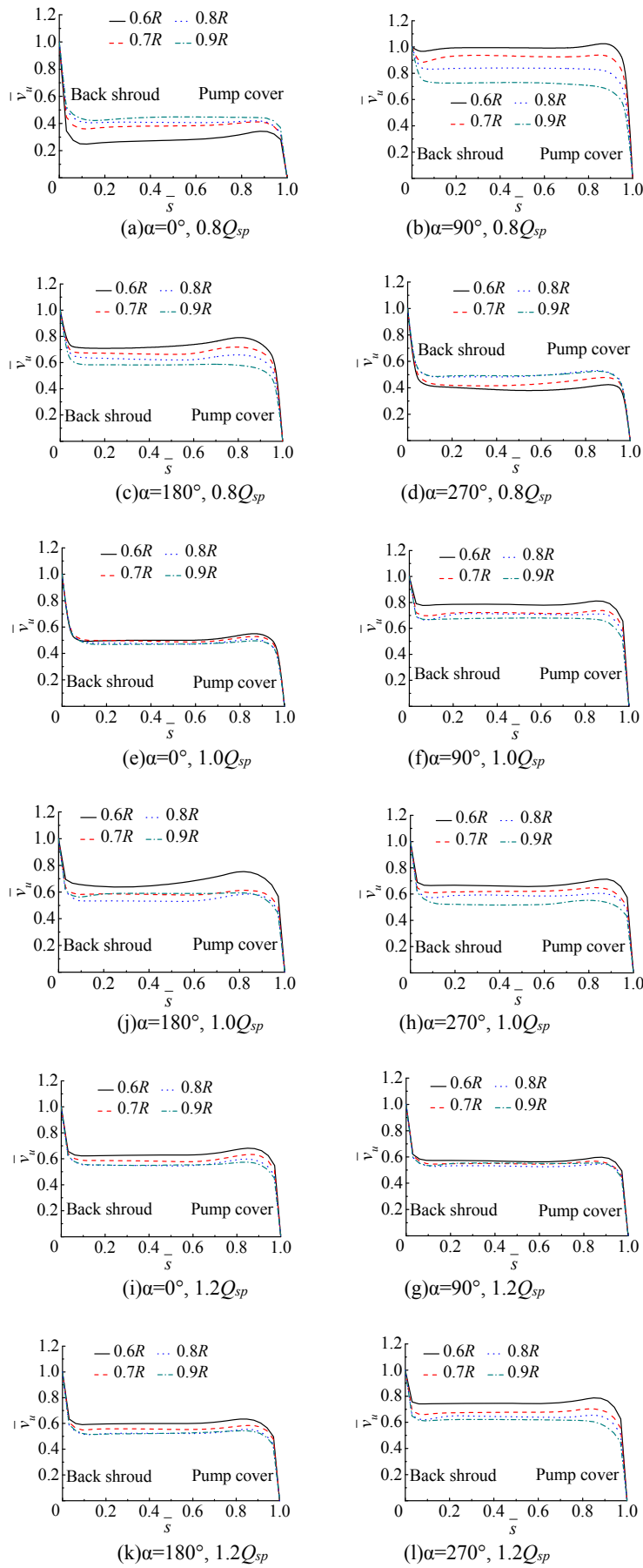


Fig. 7. Axial distribution of dimensionless tangential velocity component in the back shroud cavity.

the core zone. At the angles of 0° , 90° , 180° , and 270° (in the circumferential direction) with the same radius, the circumferential velocity in the core zone is relatively large in the direction of 90° and 180° and is smaller in the directions 0° and 270° . At the high-flow operating point ($1.2 Q_{sp}$), the kinetic energy is larger due to the lower differential pressure between the sealing ring and the volute leads to a reduction of the pressure potential energy in the direction of the larger sectional area of the volute (in the directions of 0° and 270°). The radii are 0.6, 0.7, 0.8, and 0.9 R , the circumferential velocity in the core zone is significantly larger, and the circumferential velocity in the core zone has certain radial distribution differences. Moreover, the kinetic energy of the fluid in the direction of the smaller sectional area of the volute (in the directions of 90° and 180°) is smaller than the kinetic energy in the direction of the larger sectional area, but the pressure potential energy is higher than that in the direction of the larger sectional area. Non-significant differences were observed in the radial distribution of the circumferential velocity in the core zone with the radii of 0.6, 0.7, 0.8, and 0.9 R and in the directions of 90° and 180° . These results indicate that the sectional area of the volute directly affects the flow rate of the fluid in the back shroud cavity, producing relatively significant restrictive effects on the fluid flow in the back shroud cavity.

In Fig. 7, the axial range at the turbulent boundary layers of fluid in the back shroud cavity on the back shroud face of the impeller is small compared with the core area of the flow. Certain differences exist between the rotational speed of the impeller and the circumferential velocity of the mainstream in the back shroud cavity with velocity gradients, resulting in a disc friction loss on the impeller face. When the flow rate increases from $0.8 Q_{sp}$ to $1.2 Q_{sp}$, the differential pressure between the sealing ring and the volute gradually diminishes. When the pressure potential energy on the larger sectional area of the volute in the directions of 0° and 270° significantly decreases, the kinetic energy increases. With the same radius and with less difference from the rotational speed of the impeller, the circumferential velocity in the core zone increases, and the lower disc friction decreases. In the direction of 180° , the sectional area of the volute is relatively smaller and is less affected by the mainstream inside the volute. With the same radius, however, the circumferential velocity in the core zone remains unchanged. Meanwhile, in the direction of 90° , the fluid flow inside is restricted by the volute tongue because it has the smallest sectional area of the volute; the fluid flow also undergoes a reduction in the kinetic energy and an increase in the pressure potential energy. Hence, with the same radius, the circumferential velocity in the core zone decreases because of the more significant differences in the rotational speed of the impeller and the greater disc friction loss. The fluid in the back shroud cavity is still distributed as an approximate rigid body. At the operating point with the design

flow of $1.0 Q_{sp}$, the circumferential velocity in the back shroud cavity ($0.6\text{--}0.9 R$) by four different angles is $0.46\text{--}0.79$, and the angular velocity of fluid in the back shroud cavity is $0.46\text{--}0.79$ times that of the angular velocity of the impeller. At the low-flow operating point ($0.8 Q_{sp}$), significant differences are observed between the circumferential and radial distributions of the circumferential velocity in the core zone of fluid in the back shroud cavity; this phenomenon results in significant differences in the disc friction loss by different angles or radii. In addition, at the high-flow operating point ($1.2 Q_{sp}$), fewer differences are observed between the circumferential and radial distributions of the circumferential velocity in the core zone of fluid in the back shroud cavity. The disc friction loss in the entire cavity therefore remains the same regardless of different angles or radii. Therefore, when the flow rate increases from $0.8 Q_{sp}$ to $1.2 Q_{sp}$, the disc friction loss on the impeller face inside the back shroud cavity tends to be more circumferentially or radially equal.

In Fig. 8, at operating points of the same flow rate, given that the fluid in the back shroud cavity is influenced by the joint actions of the centrifugal force and the Coriolis force, with the same angle and different radii of 0.6, 0.7, 0.8, and 0.9 R , the radial velocity in the core zone has certain differences in the axial distribution. The Coriolis force on the fluid in the back shroud cavity is closely related to the sectional area of the volute; thus, significant differences are observed in the radial distribution of the radial velocity in the core zone with the same radius and different angles of 0° , 90° , 180° , and 270° . The sectional area of the volute is particularly small in the direction of 90° , and the fluid restricts the radial flow at the tongue forms a radial pressure differential; thus, the radial velocity in the core zone is less than zero in several areas with radial leakage flow, that is, the flow in the direction of the sealing ring. With the same angle and radius, the rotational speed of the impeller face under the centrifugal force brings the radial component of velocity near the impeller cap down to greater than zero but has only a slight effect on the radial component of velocity near the pump cover that is distant from the impeller cap. Considering that the pump cover is stationary, the radial component of velocity near the pump cover is significantly less than zero and has an absolute value greater than the core zone. This result indicates that a radial leakage flow occurs in the back shroud cavity and is near the boundary layer on the pump cover.

In addition, Fig. 8 shows that the fluid in the rear pump cavity radial velocity on the turbulent boundary layer changes significantly with angle and radius. On the other hand, the radial leakage flow from the seal ring clearance forms a stable fluid flow inside the cavity and results in the uneven distribution of radial component of velocity inside the cavity. When the flow rate increases

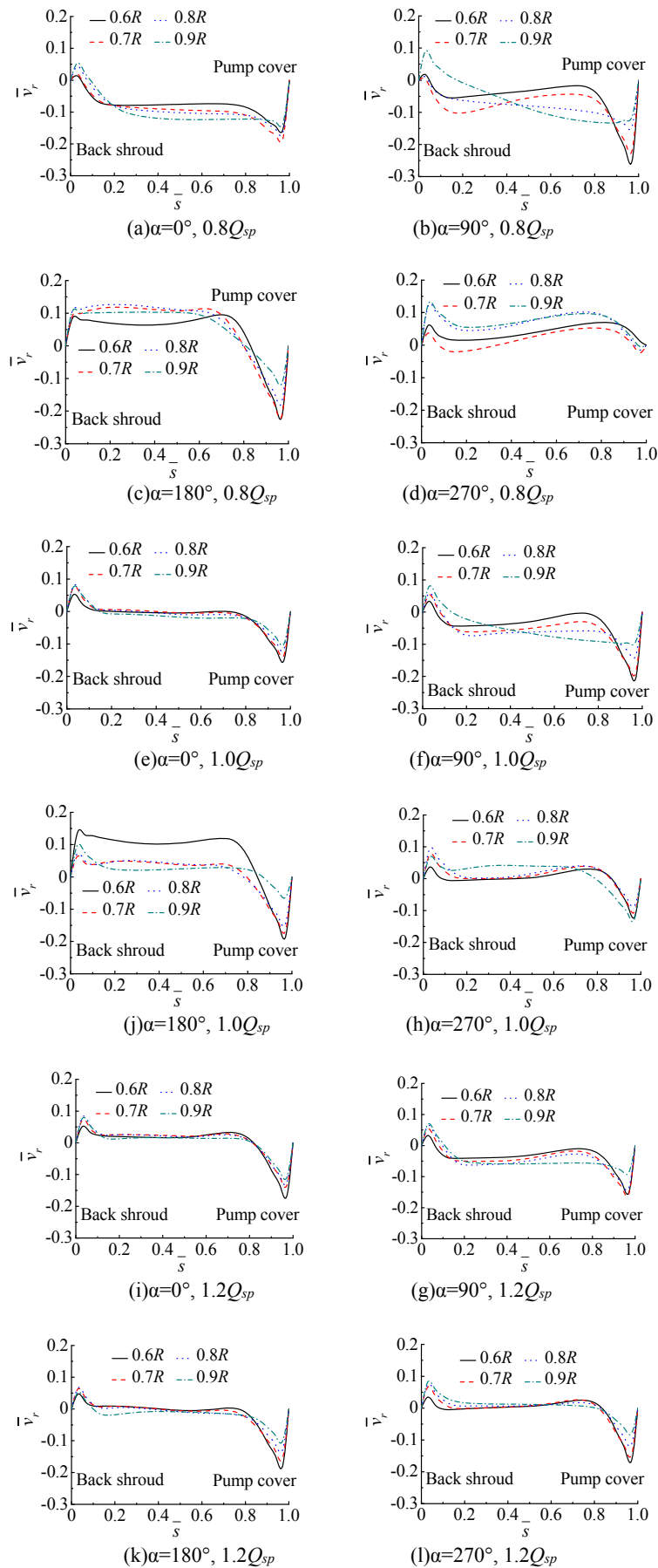


Fig. 8. Axial distribution of dimensionless radial velocity component in the back shroud cavity.

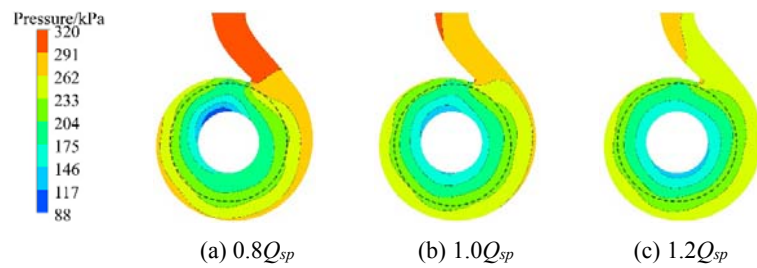


Fig. 9. Distribution of pressure in the back shroud cavity and volute.

from $0.8 Q_{sp}$ to $1.2 Q_{sp}$, these figures are less different in the distribution of the radial velocity in the core zone with the same angle and radii of 0.6, 0.7, 0.8, and 0.9 or with the same radius and the angles of 0° , 90° , 180° , and 270° ; furthermore, the value range gradually approaches zero. On the turbulent boundary layer inside the back shroud cavity close to the pump cover face, the area in which the radial velocity in the radial directions of 90° and 180° is smaller than zero and is reduced. This result indicates that when the flow rate is lower, the lower radial differential pressure induces a lower radial leakage rate in the back shroud cavity.

In the above analysis, the fluid flow in the back shroud cavity comprises the circumferential shear flow and the radial differential pressure flow, where the former originated from, the impeller cap face rotates at the rate speed, but the pump cover face remains stationary, and their relative motions cause the fluid in the back shroud cavity to form a shear flow circumferentially, where the latter originated from. A radial differential pressure occurs between the volute and the back sealing ring, forming a leakage flow from the back sealing ring clearance and causing the fluid in the back shroud cavity to flow radially because of a differential pressure. The above leakage flow can be considered as a 2D viscous laminar flow (Liu *et al.* 2013). Thus, the research findings in this paper conform to the actual flow pattern inside the pump, and these findings are highly reliable.

4.3 Analysis and Verification of Pressure Distributions

The fluid pressure distribution in the back shroud cavity is further analyzed to verify the above assertion. Figure 9 provides the fluid pressure distributions in the volute and the back shroud cavity along the axial central section of the pump cover at the operating points with the flow rates of 0.8, 1.0, and $1.2 Q_{sp}$ while considering that the fluid pressure in the volute and the back shroud cavity remains axially unchanged.

Figure 9 shows that when the flow rate increases from $0.8 Q_{sp}$ to $1.2 Q_{sp}$, the differential pressure in the volute and the back shroud cavity decreases slowly and has fewer pressure gradients. The fluid

pressure in the back shroud cavity is lower, and the pressure is more uniformly distributed along the tangential direction. At a same flow rate, the fluid pressure in the back shroud cavity increases radially from the inner diameter of the cavity to the outer diameter, whereas the pressure inside the back shroud cavity is distributed non-uniformly along the tangential direction, especially at the volute tongue where the fluid pressure is significantly stronger. This phenomenon occurs because the fluid inside the back shroud cavity is affected by the volute shape and the impeller rotation forms an asymmetric flow. However, the volute tongue produces certain restraining effects on the fluid flow, resulting in a sudden rise of the pressure at the volute tongue and a non-axially symmetric fluid pressure distribution in the back shroud cavity. This result indicates that the fluid in the back shroud cavity produces a clearance leakage flow that mainly comprises the circumferential shear flow and the radial differential pressure flow. This flow is considered as a 2D viscous laminar flow. Likewise, this result indicates that calculating the overcurrent zone between the cavity and the volute by the coupling surface is correct.

In (Chen 2005), pressure taps are set at the radii of the pump cover ($r_1=155$ mm, $r_2=130$ mm, and $r_3=110$ mm) on the closed test bench for the horizontal axial-suction pump to test the fluid pressure in the back shroud cavity of the centrifugal pump. An LWGY-DN150 intelligent turbine flowmeter is used to measure the flow rate in real time. The pressure inside the back shroud cavity is measured using a YB-150 standard pressure gauge (0.5) connected to the pressure tap in the pump cover. The pressure inside the back shroud cavity is measured at operating points of different flow rates. The experimental scheme and the specific procedures are detailed in (Chen 2005), and the designed pressure-measuring method in the back shroud cavity is depicted in Fig. 2.

The work area with the flow rate of $0.8-1.2Q_{sp}$ is considered, the mean fluid pressure in the axial geometrical center of the back shroud cavity is numerically simulated with the radii ($r_1=155$ mm, $r_2=130$ mm, and $r_3=110$ mm), and four angles of 0° , 90° , 180° , and 270° are utilized to accurately reflect the pressure inside the numerical simulation

results of the back shroud cavity and the superiority of the numerical simulation compared with the experimental test. The results are validated with the experimental test results, as shown in Fig. 10.

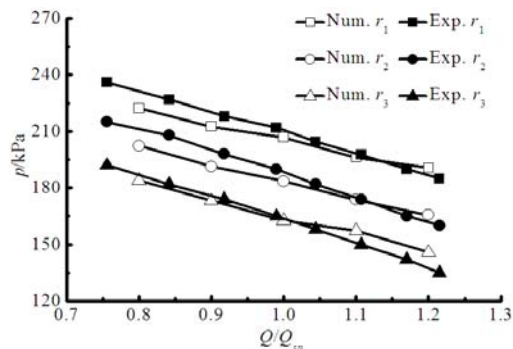


Fig. 10 Comparison of computational and experimental results of pressure in the back shroud cavity.

In Fig. 10, with the same flow rate, the fluid is affected by the differential pressure between the inner diameter and the outer diameter of the cavity. The simulated or tested pressure inside the cavity increases with radius, and the pressure curves at the three radii show a parallel distribution with the changing flow rate. The computational domain model established in this paper considers any leakage flow loss from the sealing ring clearance given that the fluid flow in the back shroud cavity under the low-flow condition is more complex than that under the high-flow condition. In addition, the relative errors between the numerical simulation and the experimental test in the disc friction loss and leakage flow loss cause larger relative errors between the simulation results and the experimental test results in the pressure at the three radii of the back shroud cavity under the low-flow condition. Smaller relative errors are observed under the high-flow condition, but a similar overall changing trend occurred at the operating point with the designed flow. At the radii of the back shroud cavity (155, 130, and 110 mm), the relative errors between the simulated values and the tested values are 2.42%, 3.37%, and 1.39%. These figures indicate that, in this paper, the measured fluid flow characteristics in the back shroud cavity of centrifugal pump impeller are accurate and reliable.

5. CONCLUSIONS

- (1) The fluid flow in the back shroud cavity characterized by circumferential shear flow and radial differential pressure flow can be considered as a 2D viscous laminar flow.
- (2) With the same flow rate, the cross-sectional area of the volute directly affects the flow rate of the fluid in the back shroud cavity, significantly restricting the fluid flow in the back shroud cavity. However, the flow pattern in the

turbulent boundary layer is greatly affected by the leakage flow; hence, the flow pattern is axially asymmetric.

- (3) From low flow to high flow, the disc friction loss of impeller-to-wall inside the back shroud cavity tends to be more circumferentially or radially equal with lower the radial differential pressure between the sealing ring and the volute; the radial leakage rate in the back shroud cavity also decreases.

ACKNOWLEDGMENT

This work supported by Research Program supported by the National Natural Science Foundation of China (Grants Nos. 51269010 and 51236006).

REFERENCES

- Benigni, H., H. Jaberg, H. Yeung, T. Salisbury, O. Berry and T. Collins (2012). Numerical simulation of low specific speed american petroleum institute pumps in part-load operation and comparison with test rig results. *Journal of Fluids Engineering*. 134(2), 024501-1-024501-9.
- Chen, Y. F (2005). *The research of pressure distribution rule in the chamber of centrifugal pump*. Master's thesis, Lanzhou University of Technology.
- Dong, W. and W. L. Chu (2016). Numerical analysis and validation of fluid pressure in the back chamber of centrifugal pump. *Journal of Mechanical Engineering*. 52(4), 165-170.
- Guan, X. F. (2011). *Theory and design of modern pump*. China Astronautic Publishing House.
- Gülich, J. F. (2003). Disk friction losses of closed turbomachine impellers. *Forschung im Ingenieurwesen / Engineering Research*. 68(2), 87-95.
- Itoh, M., Y. Yamada, S. Imao and M. Gonda (1992). Experiments on turbulent flow due to an enclosed rotating disk. *Experimental Thermal and Fluid Science*. 5(3), 359-368.
- Lefor, D., J. Kowalski, B. Kutschelis, T. Herbers and R. Mailach (2014). Optimization of axial thrust balancing swirl breakers in a centrifugal pump using stochastic methods. In *Proceeding of the ASME 2014 4th Joint US-European Fluid Engineering Division Summer Meeting*, FEDSM2014-21262.
- Lino, T., H. Sato and H. Miyashiro (1980). Hydraulic axial thrust in multistage centrifugal pumps. *Journal of Fluids Engineering*. 210(3), 163-174.
- Liu, Z. L., L. Z. Xu, X. Jia, J. Wu and D. W. Wang (2013). Analysis of liquid flow and axial force

- calculation in axial clearance for floating impeller of centrifugal pump, *Transactions of the Chinese Society of Agricultural Engineering*, 29(12), 79-85.
- Mou, J. G., S. Li, S. H. Zheng, J. B. Jin, M. Y. Su and Y. P. Zhao (2010). Influence of interstage leakage on the axial force of the multistage centrifugal pump. *Transactions of the Chinese Society for Agricultural Machinery*. 41(7), 40-44.
- Pan, D. Y., T. Wang, B. Zhang and Y. Hua (2009). PIV measurement on rotating disks flow in cylinder. *Chinese Journal of Hydrodynamics*. 24(2), 200-206.
- Park, S. H. and G. L. Morrison (2009). Analysis of the flow between the impeller and pump casing back face for a centrifugal pump. In *Proceeding of the ASME 2009 Fluids Engineering Division Summer Meeting*, 221-235.
- Shimura, T., S. Kawasaki, M. Uchiyumi and T. Kimura and J. Matsui (2012). Internal flow and axial thrust balancing of a rocket pump. *Journal of Fluid Engineering*. 134(4), 041103-1-041103-8.
- Verba, A. and G. Sebestyem (1966). Contribution to the calculation of axial thrust of multistage pumps. *Pumps in Power Stations*. 98(5), 23-34.
- Wang, X. Y., C. X. Wang and Y. B. Li (2009). Numerical study of flow characteristics in the impeller side chamber of centrifugal pump. *Transactions of the Chinese Society for Agricultural Machinery*. 40(4), 86-90.
- Yang, J. H., C. L. Wang and J. P. Li (2003). Mathematical model of flow inside a centrifugal pump casing. *Transactions of the Chinese Society for Agricultural Machinery*. 34(6), 68-72.